Ab initio study of high-lying doubly excited states of helium in static electric fields: Complex-scaling generalized pseudospectral method in hyperspherical coordinates

John Heslar[1] and Shih-I Chu[1,2]

[1]*Center for Quantum Science and Engineering, Department of Physics, National Taiwan University, Taipei 10617, Taiwan*

[2]*Department of Chemistry, University of Kansas, Lawrence, Kansas 66045, USA*

(Received 22 November 2011; published 21 September 2012)

We present a complex-scaling (CS) generalized pseudospectral (GPS) method in hyperspherical coordinates (HSC) for *ab initio* and accurate treatment of the resonance energies and autoionization widths of two-electron atomic systems in the presence of a strong dc electric field. The GPS method allows nonuniform and optimal spatial discretization of the two-electron Hamiltonian in HSC with the use of only a modest number of grid points. The procedure is applied for the first precision calculation of the energies and autoionization widths for the high-lying $^1S^e$, $^1P^o$, $^1D^e$, and $^1F^o$ ($n = 10$–20) doubly excited resonance states of He atoms. In addition, we present a theoretical prediction of the energies and widths of high-lying doubly excited resonance states of $^1P^o$ ($n = 8$–15) in external dc electric field strengths of 3.915–10.44 kV/cm. The calculated dc-field perturbed high-lying resonance energies are in good agreement with the latest experimental data.

DOI: 10.1103/PhysRevA.86.032506 PACS number(s): 31.15.ac, 32.80.Zb, 31.15.vj

I. INTRODUCTION

The helium atom is the simplest two-electron three-body system that has been studied extensively both theoretically and experimentally since the first experiment by Madden and Codling on doubly excited states in 1963 [1]. From an excitation energy of 57 eV to the He^+ $N = 2$ threshold at 65.4 eV, the spectrum of helium contains a number of Rydberg series of autoionizing states embedded in the He^+ $1s\epsilon l$ continuum. Due to the existence of strong electron-electron correlation, higher members of the Rydberg series cannot be described by the single-configuration or mean-field approximation. Numerous theoretical investigations have improved our understanding of the *e*-*e* correlation and the determination of the autoionizing resonances of the double-excited states of He in the last few decades [2]. In addition to fundamental interest, the energies, lifetimes, and oscillator strengths of these doubly excited resonance states are also of significance in astrophysics and plasma physics [3]. More recently there is considerably experimental [4–7] and theoretical [8–11] interest in the study of the effect of static electric fields on low-lying ($n \leqslant 8$) doubly excited states of helium atoms below the $N = 2$ threshold. The presence of the dc electric field allows the exploration of new sets of doubly excited states which cannot be accessed by photoexcitation directly. In this work, we present field-free theoretical prediction of high-lying doubly excited resonance states ($n = 10$–20) as well as $^1P^o$ ($n = 8$–15) series doubly excited resonance states in external dc electric fields.

The first observation of the effect of dc electric field on the photoexcitation spectrum of He doubly excited states was performed by Harries *et al.* [4], who measured the Stark shifts and splittings in strong dc fields (up to 84.4 kV/cm) in the region of the $6a - 8a$ $^1P^o$ resonances below the $N = 2$ threshold. Most theoretical works in the recent past have dealt with dc fields in this strong field regime [8–10,12]. With the exception of the dipole allowed $^1P^o$ states, most doubly excited states of He are not accessible by simple photoexcitation. In the presence of external dc electric fields, these dark states become accessible by means of the Stark mixing with the $^1P^o$ states. For example, the even $^1P^e$ series of doubly excited states have been recently observed and measured [6,11] in weak dc electric fields ($F < 10$ kV/cm). In addition, a dramatic electric field effect has been also reported in the fluorescence yield spectrum of the doubly excited states in He in the weak dc electric field regime (∼few kV/cm) [5,6,13]. To our knowledge, however, the study of the resonance energies and autoionization widths of *higher-lying* doubly excited states ($n > 10$) in the presence of dc electric fields has not yet been achieved by either experimental or theoretical methods. In this paper, we advance this field by presenting a computational method, the complex-scaling (CS) generalized pseudospectral (GPS) method in hyperspherical coordinates (HSC), for accurate treatment of high-lying doubly excited resonance states ($n = 8$–20) in the field-free case and in the presence of external dc electric fields.

The CSGPS method was first introduced for the precision study of atomic resonance states [14,15] of effective one-electron systems in spherical coordinates. The GPS method has been later extended to the time domain [16,17], allowing accurate treatment of multiphoton ionization (MPI), above-threshold ionization (ATI), and high-order harmonic generation (HHG) of atoms [16,18–20] and diatomic molecules [17,21–23] in intense laser fields by means of *self-interaction-free*, time-dependent density-functional theory [24]. The CS-GPS method has been also used in conjunction with the non-Hermitian generalized Floquet formalisms [25,26] for the accurate treatment of complex quasienergy eigenvalues and eigenfunctions associated with the MPI/HHG processes. In this paper, we extend the CSGPS method to the hyperspherical coordinates (HSC), allowing the accurate treatment of electron correlation and the effect of dc electric field on the energies and autoionization rates of Rydberg doubly excited resonance states. Our results for doubly excited states are in excellent agreement with available experimental and theoretical data. In addition, some results for high-lying resonances are presented.

The paper is organized as follows. In Sec. II, we present the CS-GPS-HSC procedure for the accurate treatment of doubly

excited resonance states in two-electron atomic systems. Section III presents the calculations of the field-free doubly excited states and the effect of dc electric field on the high-lying doubly excited resonance states. Explorations of the effects of electron correlation and doubly excited states in dc electric field are discussed in detail. Conclusions and remarks are presented in Sec. IV.

II. THEORETICAL METHOD

A. The complex-scaling generalized pseudospectral method in hyperspherical coordinates

The complex-scaling generalized pseudospectral (CSGPS) method was first introduced in 1993 for the study of atomic resonance states [14,15] in grid representation. The CSGPS approach employs the use of nonuniform and optimal spatial grid discretization of the coordinates and Hamiltonian, allowing high-precision and efficient calculation of complex quasienergy eigenvalues and eigenfunctions and MPI/ATI/HHG rates with the use of only a modest number of grid points.

In this section, we present the extension of the CSGPS method in the framework of HSC for the *ab initio* treatment of doubly-excited resonance states of the two-electron atomic systems. We note that the time-dependent generalized pseudospectral (TD-GPS) method in HSC, without the use of complex-scaling transformation, has been recently developed for the treatment of double photoexcitation of He atoms in weak attosecond xuv pulses [27], as well as the study of the effect of electron correlation on HHG of helium atoms in intense laser fields [28].

We first briefly outline below the essence of the GPS-HSC formalism [28] without the use of complex-scaling transformation. The Schrödinger equation for the field-free He atoms is given by, in atomic units,

$$\left[-\frac{1}{2}\nabla_1^2-\frac{1}{2}\nabla_2^2-\frac{2}{r_1}-\frac{2}{r_2}+\frac{1}{|\mathbf{r}_1-\mathbf{r}_2|}-E\right]\psi(\mathbf{r}_1,\mathbf{r}_2)=0. \tag{1}$$

In the HSC, Eq. (1) can be transformed to the form [28]

$$\left[-\frac{1}{2}\frac{\partial^2}{\partial R^2}-\frac{1}{8R^2}+\frac{1}{2R^2}\left(-\frac{\partial^2}{\partial\alpha^2}+\frac{\hat{l}_1^2}{\cos^2\alpha}+\frac{\hat{l}_2^2}{\sin^2\alpha}\right)+\frac{C}{R}\right]\Psi = E\Psi, \tag{2}$$

where the hyperradius, $R=\sqrt{r_1^2+r_2^2}$, is a measure of the spatial size, and the hyperangle, $\alpha=\tan^{-1}(r_2/r_1)$, depicts the radial correlation. The potential energy term C is the electron-electron and electron-nucleus potentials, given by

$$C(\alpha,\theta_{12})=\frac{2Z}{\cos\alpha}+\frac{2Z}{\sin\alpha}-\frac{2}{\sqrt{1-\sin 2\alpha\cos\theta_{12}}}. \tag{3}$$

In the HSC, the two vectors $(\mathbf{r}_1,\mathbf{r}_2)$ are replaced by the six coordinates $(R,\alpha,\Omega_1,\Omega_2)$, where Ω_i $(i=1$ and $2)$ stands for the spherical angles θ_i and ϕ_i, respectively, for the ith electron.

In the CSGPS approach in HSC, only the hyperradius coordinate R needs to be complex rotated, namely,

$$R\rightarrow Re^{i\theta}, \tag{4}$$

where θ is the rotation angle. We perform next the algebraic mapping from R to x and from α to y:

$$R(x)=L\frac{1+x}{1-x+\gamma}e^{i\theta}, \tag{5}$$

and

$$\alpha(y)=\frac{\pi}{4}(1+y), \tag{6}$$

where $\gamma=2L/R_{\max}$, and $x\in[-1,1]$, $y\in[-1,1]$, $R\in[0,R_{\max}]$, $\alpha\in[0,\pi/2]$, and L is the mapping parameter. The variables x and y are discretized using the Gauss-Legendre abscissas x_i and y_j as the collocation points. The given space that the two electrons are confined to is determined by the size of $R_{\max}$ [14].

Under the complex-scaling transformation, Eq. (2) becomes

$$\left[-\frac{e^{-i2\theta}}{2}\frac{\partial^2}{\partial R^2}-\frac{e^{-i2\theta}}{8R^2}+\frac{e^{-i2\theta}}{2R^2}\left(-\frac{\partial^2}{\partial\alpha^2}+\frac{\hat{l}_1^2}{\cos^2\alpha}+\frac{\hat{l}_2^2}{\sin^2\alpha}\right)+\frac{Ce^{-i\theta}}{R}\right]\Psi(Re^{i\theta},\alpha,\Omega_1,\Omega_2)=\epsilon\Psi(Re^{i\theta},\alpha,\Omega_1,\Omega_2), \tag{7}$$

where ϵ denotes the complex energies of the autoionizing resonance states. We expand the total two-electron wave function Ψ in terms of the complex-scaled adiabatic channels

$$\Psi(Re^{i\theta},\alpha,\Omega_1,\Omega_2)=\frac{e^{-i\frac{5}{2}\theta}}{R^{\frac{5}{2}}\sin\alpha\cos\alpha}\sum_\mu F_\mu(Re^{i\theta})\times\Phi_\mu(Re^{i\theta},\alpha,\Omega_1,\Omega_2), \tag{8}$$

where $F_\mu(Re^{i\theta})$ is to be solved in the hyperradius space, and the adiabatic channel functions $\Phi_\mu(Re^{i\theta},\alpha,\Omega_1,\Omega_2)$ describe the radial correlation between the two electrons [29]. These channel functions are obtained by solving the adiabatic Hamiltonian [28] at a fixed value of R:

$$H_{ad}\Phi_\mu(Re^{i\theta},\alpha,\Omega_1,\Omega_2)=U_\mu(Re^{i\theta})\Phi_\mu(Re^{i\theta},\alpha,\Omega_1,\Omega_2). \tag{9}$$

Here the channel functions $\Phi_\mu(Re^{i\theta},\alpha,\Omega_1,\Omega_2)$ can be represented in a way to satisfy the exchange symmetry ${}^{2S+1}L^\pi$, $(\pi=e$ or $o)$ for either singlet or triplet states, and they can be expanded in terms of two-particle spherical harmonics $\mathcal{Y}_{l_1l_2}^{LM}(\Omega_1,\Omega_2)$ [27]. For fixed L, M, S, and π, we have

$$\Phi_\mu^{L,l_1,l_2}(Re^{i\theta},\alpha,\Omega_1,\Omega_2)=\begin{cases}\frac{1}{\sqrt{2}}\sum_{l_1l_2}\left[f_\mu^{L,l_1,l_2}(Re^{i\theta},\alpha)\mathcal{Y}_{l_1,l_2}^{LM}(\Omega_1,\Omega_2)+(-1)^A f_\mu^{L,l_2,l_1}\left(Re^{i\theta},\frac{\pi}{2}-\alpha\right)\mathcal{Y}_{l_2,l_1}^{LM}(\Omega_1,\Omega_2)\right], & l_1\neq l_2,\\ \sum_{l_1l_2}f_\mu^{L,l_1,l_2}(Re^{i\theta},\alpha)\mathcal{Y}_{l_1,l_2}^{LM}(\Omega_1,\Omega_2), & l_1=l_2,\end{cases} \tag{10}$$

where we define $A = l_1 + l_2 - L + S$. L and S are the total orbital and spin angular momenta, and M and π denote the magnetic quantum number and parity of the total orbital angular momentum, respectively. In Eq. (10), the coefficients $f(Re^{i\theta},\alpha)$ are the cardinal functions at those Gauss-Legendre quadrature points [16].

Once the adiabatic eigenvalue problem is solved [Eq. (9)], we then use these complex-scaled channel functions to compute the coupling terms [29] and the overlap matrix elements,

$$\mathcal{O}_{i\mu,j\mu'} = \langle \Phi_\mu(R_i e^{i\theta},\alpha,\Omega_1,\Omega_2)|\Phi_{\mu'}(R_j e^{i\theta},\alpha,\Omega_1,\Omega_2)\rangle. \quad (11)$$

After making the coordinate transformations Eqs. (4)–(6), we obtain the following complex scaled wave function:

$$\begin{aligned}&\Psi(Re^{i\theta},\alpha,\Omega_1,\Omega_2)\\ &= \sqrt{R'(x)}\sum_{i=1}^{N_R} f_i(xe^{i\theta})\Psi(x_i e^{i\theta},y,\Omega_1,\Omega_2)\\ &= \sqrt{R'(x)}\sum_{i\mu}^{N_R N_\mu} f_i(xe^{i\theta})C_{i\mu}\Phi(x_i e^{i\theta},y,\Omega_1,\Omega_2), \quad (12)\end{aligned}$$

where N_R and N_μ are the number of collocation points for the hyperradius and the number of discretized channels for the adiabatic Hamiltonian, respectively. Inserting the discretized representation of Eq. (12) into Eq. (7), we can rewrite the discretized Schrödinger equation in the form

$$\begin{aligned}&\sum_{i'\mu'}[\mathcal{K}(Re^{i\theta})_{ii'}\mathcal{O}_{i\mu,i'\mu'} + \delta_{ii'}U^L_{\mu'}(R_{i'}e^{i\theta})\mathcal{O}_{i\mu,i'\mu'}]C_{i\mu}\\ &= \epsilon\sum_{i'\mu'}\mathcal{O}_{i\mu,i'\mu'}C_{i\mu}, \quad (13)\end{aligned}$$

where $\mathcal{K}(Re^{i\theta})_{ii'}$ represents the complex-scaled kinetic energy matrix elements, and $U^L_{\mu'}(R_{i'}e^{i\theta})$ is the complex-scaled adiabatic eigenenergy at each $R_{i'}$ for the corresponding L and adiabatic channel μ'.

The first advantage in the present CSGPS-HSC procedure is that the GPS method is a nonlinear grid discretization method. This ensures that the short-range part of the Coulomb interaction is properly represented. Therefore, a denser portion of grid points is distributed near the origin. The second advantage is that, in the CSGPS approach, the complex-rotated coordinate R is discretized on a set of collocation grid points. The potential matrix elements are diagonal, and equal to the values of the potential at the grid points. The kinetic energy matrix elements $\mathcal{K}(Re^{i\theta})_{ii'}$ in Eq. (13) have simple explicit analytical expressions. This speeds up the numerical calculation considerably and at the same time provides highly accurate wave functions at the grid points.

III. RESULTS AND DISCUSSIONS

A. Determination of the energies and autoionization widths for high-lying doubly excited resonance states

In this section, we present our calculated resonance energies and autoionization (half) widths for the high-lying doubly-excited resonance states (n = 10–20) of the He atom below the $N = 2$ threshold in Tables I–IV. We also compare our results of $^1S^e$, $^1P^o$, $^1D^e$, and $^1F^o$ Rydberg states with other recent theoretical data [30–33]. The agreement is generally excellent for the doubly excited states up to n = 10–15. To our

TABLE I. The calculated resonance energies E_r and autoionization (half) widths $\Gamma/2$ for the n = 10–20 doubly-excited Rydberg states $^1S^e$ $(2,n,(a,b))$ below the $N = 2$ threshold (in a.u.). Numbers in square brackets indicate powers of ten.

	State	$-E_r$	$\Gamma/2$	State	$-E_r$	$\Gamma/2$
Present	10*a*	0.505759011	9.777[−6]	10*b*	0.504746220	2.775[−6]
[30]		0.505759052	9.777[−6]		0.504746230	2.776[−6]
[31]		0.505759104	9.790[−6]		0.504746388	2.766[−6]
Present	11*a*	0.504697225	7.131[−6]	11*b*	0.503940604	2.145[−6]
[30]		0.504697299	7.131[−6]		0.503940615	2.146[−6]
[32]		0.504697187	7.131[−6]			
Present	12*a*	0.503904116	5.362[−6]	12*b*	0.503324068	1.700[−6]
[30]		0.503904132	5.362[−6]		0.503324031	1.690[−6]
[32]		0.503904047	5.360[−6]			
Present	13*a*	0.503296014	4.134[−6]	13*b*	0.502841616	1.350[−6]
[30]		0.503296078	4.134[−6]		0.502841626	1.350[−6]
[32]		0.503296011	4.131[−6]			
Present	14*a*	0.502819664	3.251[−6]	14*b*	0.502457209	1.137[−6]
[30]		0.502819726	3.253[−6]		0.502457222	1.136[−6]
[32]		0.502819669	3.239[−6]			
Present	15*a*	0.502439597	2.613[−6]	15*b*	0.502145509	8.058[−7]
[30]		0.502439676	2.617[−6]		0.502145517	8.06[−7]
[32]		0.502439599	2.689[−6]			
Present	16*a*	0.502131622	2.090[−6]	16*b*	0.501889058	5.817[−7]
Present	17*a*	0.501878528	1.681[−6]	17*b*	0.501676589	4.910[−7]
Present	18*a*	0.501666988	1.452[−6]	18*b*	0.501498052	4.181[−7]
Present	19*a*	0.501489971	1.274[−6]	19*b*	0.501346589	3.647[−7]
Present	20*a*	0.501341721	1.179[−6]	20*b*	0.501216515	3.082[−7]

TABLE II. The calculated resonance energies E_r and autoionization (half) widths $\Gamma/2$ for the $n = 10$–20 doubly-excited Rydberg states $^1P^o$ $(2,n,(a,b,c))$ below the $N = 2$ threshold (in a.u.). Numbers in square brackets indicate powers of ten.

	State	$-E_r$	$\Gamma/2$	State	$-E_r$	$\Gamma/2$	State	$-E_r$	$\Gamma/2$
Present	10a	0.505174452	4.052[−6]	10b	0.505806734	4.90[−8]	10c	0.504758332	8.15[−11]
[30]		0.505174494	4.054[−6]		0.505806870	4.9[−8]		0.504758391	
[34]		0.505175	4[−6]		0.50580696	1.0[−7]		0.5047590	
Present	11a	0.504259181	3.031[−6]	11b	0.504732042	3.62[−8]	11c	0.503950110	6.08[−11]
[30]		0.504262710	3.038[−6]		0.504732057	3.6[−8]		0.503950219	
Present	12a	0.503572206	2.332[−6]	12b	0.503930196	2.79[−8]	12c	0.503331700	3.31[−11]
[30]		0.503572348	2.335[−6]		0.503930208	2.8[−8]		0.503331706	
Present	13a	0.503037023	1.829[−6]	13b	0.503316098	2.09[−8]	13c	0.502847463	1.51[−11]
[30]		0.503037093	1.834[−6]		0.503316151	2.1[−8]		0.502847834	
Present	14a	0.502613680	1.432[−6]	14b	0.502835501	1.54[−8]	14c	0.502462316	0.72[−11]
[30]		0.502613741	1.434[−6]		0.502835510	1.5[−8]		0.502462325	
Present	15a	0.502273019	1.332[−6]	15b	0.502452286	3.88[−8]	15c	0.502149624	0.15[−11]
[30]		0.502273028	1.335[−6]		0.502452349	3.9[−8]		0.502149666	
Present	16a	0.501993794	9.535[−7]	16b	0.502140336	1.04[−8]	16c	0.501892145	0.77[−12]
Present	17a	0.501763954	7.939[−7]	17b	0.501885535	8.03[−9]	17c	0.501679199	0.45[−12]
Present	18a	0.501571686	6.680[−7]	18b	0.501673666	6.31[−9]	18c	0.501500276	0.33[−12]
Present	19a	0.501409224	5.674[−7]	19b	0.501495600	4.06[−9]	19c	0.501348498	0.17[−12]
Present	20a	0.501270711	4.859[−7]	20b	0.5013445104	2.29[−9]	20c	0.501218639	0.09[−12]

knowledge, there is currently no experimental or theoretical data in the higher-lying resonance states ($n > 15$) available. In the present work, we extend our CSGPS-HSC study to the higher-lying doubly excited resonance states ($n = 15$–20), which are also shown in Tables I–IV. Throughout this paper, we use the (N,n, (a,b, or c)) representation for doubly excited states introduced by Lipsky and Conneely [35], which is widely used for He. We expect our results will stimulate further experimental works in the future.

When we incorporated ten adiabatic eigenchannels and five partial waves (l_1,l_2) in the calculation, the ground-state energy of helium is determined to be −2.903 723 a.u., in good agreement with the benchmark result of −2.903 724 a.u. [36]. In Tables I–IV, the results for all the symmetries are calculated accurately by using 20 eigenchannels and 20 partial waves (l_1,l_2), with $R_{\max} = 500$ a.u., to ensure convergency.

Our predicted results of the resonance energies by means of the CSGPS-HSC method are converged at least to 10^{-10} a.u., and the widths are converged to the digit of accuracy shown in the tables (Tables I–V) and figures (Figs. 1 and 2). We note that such an accuracy for the Rydberg resonance energies and widths by the present CSGPS-HSC procedure has not yet been achieved by the traditional basis-set expansion methods or the B-spline functions.

TABLE III. The calculated resonance energies E_r and autoionization (half) widths $\Gamma/2$ for the $n = 10$–20 doubly-excited Rydberg states $^1D^e$ $(2,n,(a,b,c))$ below the $N = 2$ threshold (in a.u.). Numbers in square brackets indicate powers of ten.

	State	$-E_r$	$\Gamma/2$	State	$-E_r$	$\Gamma/2$	State	$-E_r$	$\Gamma/2$
Present	10a	0.505328768	6.793[−6]	10b	0.505012277	4.463[−7]	10c	0.504874911	1.813[−9]
[30]		0.505328784	6.799[−6]		0.505012580	4.47[−7]		0.504874929	1[−9]
Present	11a	0.504378289	5.069[−6]	11b	0.504141604	3.377[−7]	11c	0.504038182	1.114[−9]
[30]		0.504378303	5.071[−6]		0.504141617	3.38[−7]		0.504038200	1.000[−9]
Present	12a	0.503661137	3.821[−6]	12b	0.503479422	2.622[−7]	12c	0.503399708	8.312[−10]
[30]		0.503661148	3.882[−6]		0.503479414	2.62[−7]		0.503399748	8[−10]
Present	13a	0.503106758	3.031[−6]	13b	0.502964210	2.045[−7]	13c	0.502901529	7.254[−10]
[30]		0.503106766	3.037[−6]		0.502964214	2.07[−7]		0.502901543	7[−10]
Present	14a	0.502669301	2.419[−6]	14b	0.502555489	1.598[−7]	14c	0.502505310	5.412[−10]
[30]		0.502669381	2.421[−6]		0.502555511	1.62[−7]		0.502505327	
Present	15a	0.502318297	1.931[−6]	15b	0.502225905	1.712[−7]	15c	0.502185026	3.964[−10]
[30]		0.502318305	1.939[−6]		0.502225953	1.76[−7]		0.502185075	
Present	16a	0.502119020	9.049[−7]	16b	0.502032470	7.812[−8]	16c	0.501952454	9.29[−11]
Present	17a	0.501858693	3.540[−7]	17b	0.501792102	2.904[−8]	17c	0.501720766	3.73[−11]
Present	18a	0.501614863	1.807[−7]	18b	0.501586479	1.511[−8]	18c	0.501530058	7.1[−12]
Present	19a	0.501507873	1.011[−7]	19b	0.501431527	9.255[−9]	19c	0.501401640	2.6[−13]
Present	20a	0.501348770	8.151[−8]	20b	0.501349341	7.230[−9]	20c	0.501218639	1[−13]

TABLE IV. The calculated resonance energies E_r and autoionization (half) widths $\Gamma/2$ for the $n = 10$–20 doubly-excited Rydberg states $^1F^o$ $(2,n,(a,b,c))$ below the $N = 2$ threshold (in a.u.). Numbers in square brackets indicate powers of ten.

	State	$-E_r$	$\Gamma/2$	State	$-E_r$	$\Gamma/2$	State	$-E_r$
Present	10*a*	0.505058334	2.890[−7]	10*b*	0.505016412	1.811[−10]	10*c*	0.504924432
[30]		0.505058342	2.88[−7]		0.505016428	2[−10]		0.504924466
Present	11*a*	0.504175912	2.204[−7]	11*b*	0.504144617	1.253[−10]	11*c*	0.504076210
[30]		0.504175949	2.18[−7]		0.504144611	1[−10]		0.504076225
Present	12*a*	0.503505796	1.687[−7]	12*b*	0.503481706	1.009[−10]	12*c*	0.503429022
[30]		0.503505827	1.69[−7]		0.503481779	1[−10]		0.503429075
Present	13*a*	0.502984948	1.350[−7]	13*b*	0.502966093	7.82[−11]	13*c*	0.502924588
[30]		0.502984969	1.33[−7]		0.502966109	8[−11]		0.502924637
Present	14*a*	0.502572129	1.069[−7]	14*b*	0.502557030	5.69[−11]	14*c*	0.502523827
[30]		0.502572121	1.07[−7]		0.502557054	6[−11]		0.502523838
Present	15*a*	0.502239306	7.432[−8]	15*b*	0.502227098	4.34[−11]	15*c*	0.502200108
[30]		0.502239372	7.5[−8]		0.502227191			0.502200122
Present	16*a*	0.501840336	5.024[−8]	16*b*	0.501793794	1.28[−11]	16*c*	0.501692145
Present	17*a*	0.501685535	2.077[−8]	17*b*	0.501563954	0.24[−11]	17*c*	0.501579199
Present	18*a*	0.501473666	9.314[−9]	18*b*	0.501471686	0.66[−12]	18*c*	0.501300276
Present	19*a*	0.501395600	1.243[−9]	19*b*	0.501209224	0.12[−12]	19*c*	0.501248498
Present	20*a*	0.501244510	6.222[−10]	20*b*	0.501070711	0.91[−13]	20*c*	0.501118639

Tables I–IV display (as n increases) the resonance energies converging to the He^+ $(N = 2)$ ionization thresholds (−0.5 a.u.). One of the features revealed from Tables I–IV is the common trend of the autoionization rates, which decrease as the quantum number n increases.

TABLE V. Calculated field-free and field-perturbed resonance energies E_r and autoionization (half) width $\Gamma/2$ (in a.u.) for the $n = 8$–15 doubly excited Rydberg $^1P^o$ states below the $N = 2$ threshold. Numbers in square brackets indicate powers of ten.

F (V/cm)	State	$-E_r$	$\Gamma/2$	State	$-E_r$	$\Gamma/2$
0	8*a*	0.508158278	7.9658[−6]	9*a*	0.506413702	5.572[−4]
3915		0.508129956	1.5509[−6]		0.506369923	0.1111[−4]
5438		0.508102683	1.5084[−6]		0.506356012	0.1103[−4]
6525		0.508105623	1.4753[−6]		0.506374800	0.1095[−4]
7613		0.508058225	1.4382[−6]		0.506322365	0.1087[−4]
8700		0.508061532	1.4012[−6]		0.506371772	0.1077[−4]
10440		0.508108243	1.3398[−6]		0.506344442	0.1060[−4]
0	10*a*	0.505174852	3.989[−6]	11*a*	0.504259181	3.061[−6]
3915		0.505073102	0.7176[−5]		0.504158874	0.5596[−5]
5438		0.505048006	0.6767[−5]		0.504131354	0.5119[−5]
6525		0.505022143	0.6545[−5]		0.504140882	0.4671[−5]
7613		0.504990094	0.6374[−5]		0.504057374	0.4129[−5]
8700		0.50503704	0.6243[−5]		0.504112002	0.3505[−5]
10440		0.505034226	0.6095[−5]		0.504094210	0.2448[−5]
0	12*a*	0.503569606	2.316[−6]	13*a*	0.503037923	1.796[−6]
3915		0.503476447	0.4430[−5]		0.502913832	0.1107[−5]
5438		0.503458349	0.4271[−5]		0.502776991	0.1025[−5]
6525		0.503326001	0.4131[−5]		0.502794228	0.1734[−5]
7613		0.503342662	0.3894[−5]		0.502778839	0.2987[−5]
8700		0.503317389	0.3380[−5]		0.502659111	0.4524[−5]
10440		0.503379114	0.1614[−5]		0.502692099	0.2790[−5]
0	14*a*	0.502613980	1.427[−6]	15*a*	0.502272673	1.358[−6]
3915		0.502408440	0.2247[−5]		0.502038166	0.1951[−5]
5438		0.502342324	0.1964[−5]		0.501972034	0.3615[−5]
6525		0.502254060	0.3434[−5]		0.501861343	0.1007[−4]
7613		0.502295193	0.6938[−5]		0.501847895	0.5408[−5]
8700		0.502208033	0.8642[−5]		0.501738941	0.1732[−5]
10440		0.502175043	0.2690[−5]		0.501711885	0.6170[−5]

The resonance energies and autoionization widths can be approximately parameterized by [31,37]

$$E_{2,k,n} = -1/2 - \frac{(Z-1)^2}{2(n-\mu_{kn})^2}, \tag{14}$$

where $k = a$, b, or c series for each total orbital angular momenta L and μ_{kn} is the quantum defect. Here, μ_{kn} is complex since $E_{2,k,n}$ has real and imaginary parts. The effective quantum number n^* is defined as follows:

$$n^* = n - \mathrm{Re}\mu_{kn}. \tag{15}$$

Since the autoionization widths are very small, we have $\mathrm{Im}\mu_{kn} \ll n^*$. Then we can expand the right-hand side of Eq. (14) and write down the approximate expression,

$$E_{2,k,n} \approx -1/2 - \frac{(Z-1)^2}{2(n^*)^2} - i\frac{\mathrm{Im}\mu_{kn}(Z-1)^2}{(n^*)^3}, \tag{16}$$

so the He autoionization widths can be expressed as

$$\Gamma/2 \approx \frac{\mathrm{Im}\mu_{kn}}{(n^*)^3}. \tag{17}$$

From Eq. (17), we see the decrease in the autoionization widths is approximately inversely proportional to $(n^*)^3$. The real part of the quantum defect ($\mathrm{Re}\mu_{kn}$) varies linearly with $E_{2,k,n}$ following Eqs. (14)–(17), as seen in Figs. 1 and 2 up to quantum number $n = 15$ (a and b). The imaginary part ($\mathrm{Im}\mu_{kn}$) also has a linear variation up to $n = 15$a (Fig. 1) and $n = 13$b (Fig. 2). However, our results show that at higher doubly excited states $n \geqslant 13$, the parametrized equations [Eqs. (14)–(17)] can no longer be used to describe the states as seen in Figs. 1 and 2. Similar observation has been reported earlier for the lower states. For example, we plot the data ($n \leqslant 15$) from Ref. [30] shown in Table I in Fig. 2 (red dotted curve) and similar deviations ($n = 13$–15) from linear variation are observed. In other words, they do not follow the parametrized equations Eqs. (14)–(17) either.

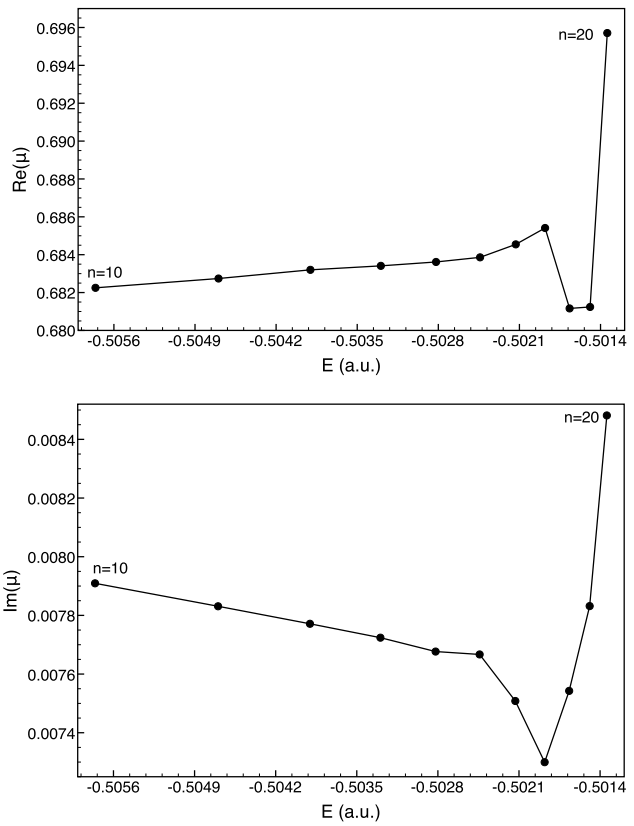

FIG. 1. Quantum defect (real and imaginary part) for the $n = 10$–20(a) $^1S^e$ doubly-excited Rydberg states below the $N = 2$ threshold.

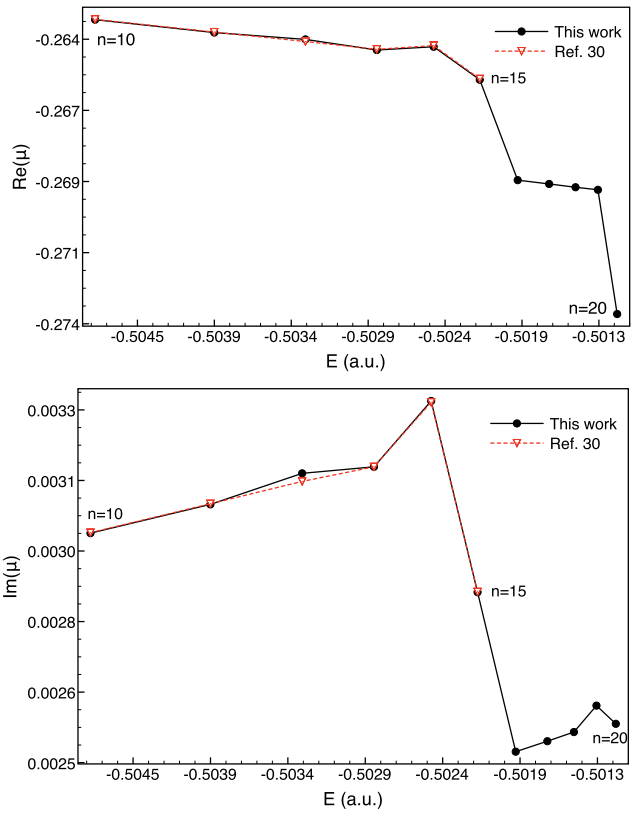

FIG. 2. (Color online) Quantum defect (real and imaginary part) for the $n = 10$–20(b) $^1S^e$ doubly-excited Rydberg states below the $N = 2$ threshold. Also shown are the results from Ref. [30] for comparison.

As another example, Wintgen *et al.* [38] used the frozen planet method (where one electron is held fixed) to calculate the resonances for $^1S^e$ and $^3S^e$ ($n \leqslant 15$) and found the quantum defect fluctuated rapidly and did not follow the linear variation trend as shown in Eqs. (14)–(17).

To our knowledge, there is no earlier published results on quantum defects for $^1S^e$ ($2,n \geqslant 15,(a,b)$) below the $N = 2$ threshold. Our results presented here represent results in this higher Rydberg regime ($n > 15$).

B. The dc Stark effects on the high-lying doubly excited resonance states

In the presence of an external dc electric field, the Hamiltonian for a two-electron atom is

$$H = H_0 + V = H_0 + \mathbf{F}(\mathbf{r}_1 + \mathbf{r}_2), \tag{18}$$

where H_0 is the field-free Hamiltonian, and $\mathbf{F}$ is the uniform external electric field in the z axis. The matrix elements of Fz_1 and Fz_2 are the same for a given pair of wavefunctions.

Here we present only the matrix element of Fz_1 explicitly as follows:

$$\left\langle \Psi_k^L \middle| F(z_1) \middle| \Psi_{k'}^{L'} \right\rangle = \frac{1}{2} F \sum_{\mu,\mu'} \sum_{l_1,l_2} \sum_{l_1',l_2'} \left[\sum_i F^L(R_i e^{i\theta}) R_i e^{i\theta} F^{L'}(R_i e^{i\theta}) \omega_i \right] \left\{ \sum_j \Phi_\mu^{l_1 l_2 L}(R_i e^{i\theta}, \alpha_j) \cos\alpha_j \Phi_{\mu'}^{l_1' l_2' L'}(R_i e^{i\theta}, \alpha_j) \right.$$

$$\left. \times \lambda_j \Theta_{l_1 l_2 L M}^{l_1' l_2' L' M'} + (-1)^A \sum_j \Phi_\mu^{l_1 l_2 L}(R_i e^{i\theta}, \pi/2 - \alpha_j) \cos\alpha_j \Phi_{\mu'}^{l_1' l_2' L'}(R_i e^{i\theta}, \alpha_j) \lambda_j \Theta_{l_2 l_1 L M}^{l_1' l_2' L' M'} \right\}, \quad (19)$$

where

$$\Theta_{l_1 l_2 L M}^{l_1' l_2' L' M'} = \left\langle \mathcal{Y}_{l_1,l_2}^{LM}(\Omega_1,\Omega_2) \middle| \cos\theta_1 \middle| \mathcal{Y}_{l_1',l_2'}^{L'M'}(\Omega_1,\Omega_2) \right\rangle. \quad (20)$$

Here ω_i and λ_j are the corresponding Gauss-Legendre weights to the hyperradial and hyperangle spatial coordinate, respectively. For states in dc field along the z direction, the total magnetic quantum number M is a conserved quantity, while the parity along the z axis (π_z) is not conserved. We will focus our attention on the $M = 0$ manifolds. Since the parity is not conserved, the angular momentum states $^1S^e$, $^1P^o$, $^1D^e$, $^1F^o$, etc. are coupled together in Eq. (19) by the external electric field. This ten-symmetry ($L_{\max} = 9$) calculation is sufficient to achieve the convergency for such doubly excited states in electric field. We investigate here the $^1P^o$ $(2,n,a,b)$ resonance states, where $n = 8$–15, in the dc electric field. We use a mesh of $N_R \times N_\alpha = 400 \times 400$, and 20 adiabatic channels ($\mu_{\max} = 20$) to compute the field-free wave functions Ψ_k^L, where $L = 0$–9. Our calculated widths are converged when the rotation angle θ is varied from 0.1 to 0.3 rad. We have tested the convergency of the calculations by including more partial waves and more grid points. For example, we have incorporated 25 partial waves (l_1,l_2), with $R_{\max} = 600$ a.u. and the test showed that the calculation was converged for all the data shown in the tables. Similarly, we have tested the convergency by adding more mesh points ($N_R \times N_\alpha = 450 \times 420$), and again the calculated results are identical to the previous results using the mesh of $N_R \times N_\alpha = 400 \times 400$.

In Table V, we present the dc electric field effects on the resonance energies and autoionization (half) widths for doubly excited Rydberg states of He, where the electric field strength is varied from 3915 to 10,440 V/cm. For the low-lying resonance states ($n = 6$) in a dc electric field strength F of 84.4 kV/cm, our results are in very good agreement with the previous theoretical and experimental data [8]. For higher-lying Rydberg resonance states ($n = 8$–15) in a dc electric field, to our knowledge, there are currently no theoretical and experimental results available. We note that experimental determination of the resonance energies and widths for such high-lying doubly excited states in the presence of electric fields are currently difficult to perform due to the limited spectral resolution and complicated peak splitting pattern [39]. Since the field-free autoionization rates in the states of interest are small to begin with, see, for example, $^1P^o 338$ $(2,10a)$ ($\Gamma = 7.987 \times 10^{-6}$ a.u.), even small electric field strength has significant effects on these doubly excited states. From Table V, we notice that the doubly excited state energies and widths are modified by the presence of the electric field, and the effect becomes stronger with increasing n.

In Figs. 3 and 4, we compare our calculated resonance energies with the fluorescence yield (FY) spectra from Såthe *et al*. [5] at various dc field strengths for the $^1P^o$ ($N = 2, n = 8$–15, a,b) series below the $N = 2$ threshold. In their work [5], they used the WKB method [40] for their theoretical calculations and comparisons with the experimental FY spectra. In Fig. 1 of Såthe *et al*. work [5], it is shown that their theoretical FY spectra (based on the WKB method [40]) are shifted in energies and deviated substantially from the experimental spectra. The WKB method assumes the Rydberg-electron wave function is purely bound, and the main physical effects are not included in the theoretical simulation in [5]. In our present fully *ab initio* CSGPS-HSC approach, the calculated resonance energies are in good agreement with the peak positions of the experimental FY spectra, as shown in Figs. 3 and 4. In Fig. 3 (bottom panel) the nb series is shown for the field-free case. Note that as the dc-electric field strength

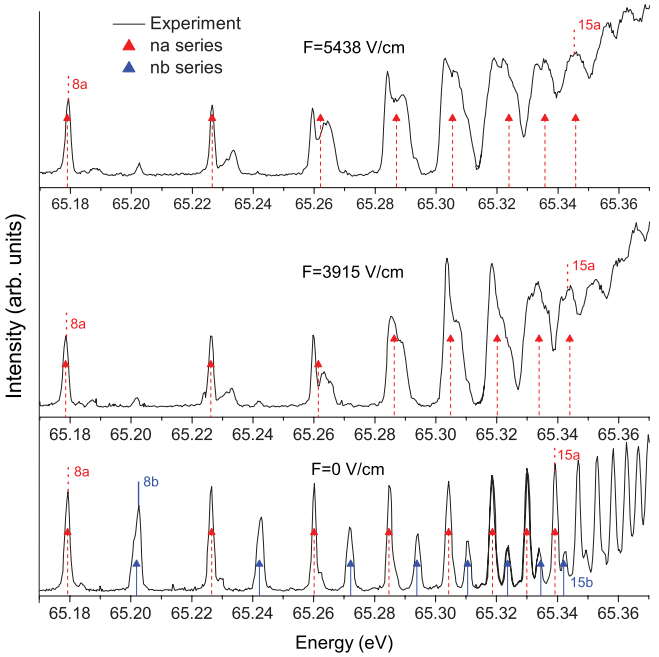

FIG. 3. (Color online) Experimental fluorescence yield spectra [5] and calculated resonance energies E_r for the $n = 8$–15(a,b) $^1P^o$ doubly excited Rydberg states below the $N = 2$ threshold in dc fields. Here the red (dashed) line and blue (solid) line correspond to (na) and (nb) series, respectively, and the peaks at the lowest energy correspond to 8(a).

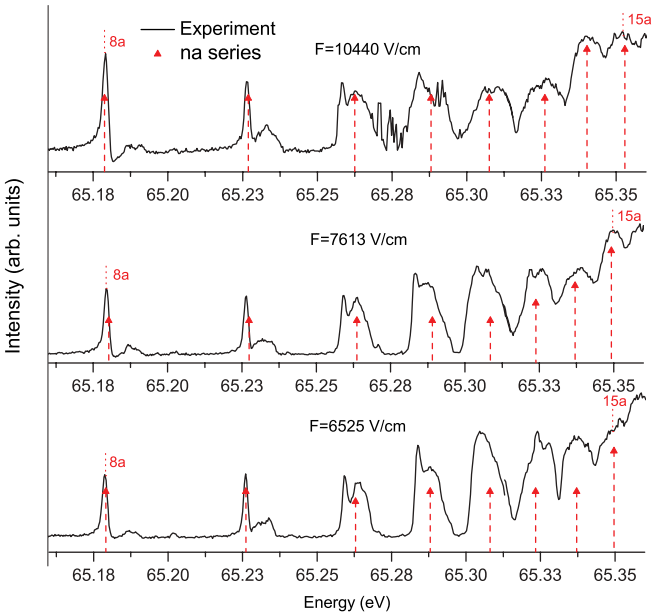

FIG. 4. (Color online) Experimental fluorescence yield spectra [5] and calculated resonance energies E_r for the $n = 8$–15(a) $^1P^o$ doubly excited Rydberg states below the $N = 2$ threshold in dc fields. Here the red dashed line corresponds to (na) series and the peaks at the lowest energy correspond to 8(a).

is increased above zero, the nb and nc series FY quickly disappear (unresolved experimentally) [5].

IV. CONCLUSION

In conclusion, we have presented a CSGPS method in hyperspherical coordinates for the accurate *ab initio* nonperturbative treatment of the resonance energies and autoionzation widths of doubly-excited high-lying resonance states of He in the field-free case and in the presence of dc-electric fields. Our theoretical predictions for low-lying resonance states are in good agreement with available theoretical and experimental data. In addition, we present results for *high-lying* resonance states which are currently difficult to achieve by either experimentally or other theoretical methods. Our CSGPS-HSC approach is shown to be capable of providing accurate resonance energies and widths for $^1S^e$, $^1P^o$, $^1D^e$, and $^1F^o$ doubly-excited Rydberg states with the use of only a modest number of grid points. The effects of dc-field on the autoionization rates for the odd-parity $^1P^o$ states where $n = 8$–15 have been identified. We hope that our presented predictions and findings will stimulate further experimental and theoretical activities in the future.

ACKNOWLEDGMENTS

We would like to thank Jan-Erik Rubensson for useful discussions and for providing us with their experimental results. This work was partially supported by the US Department of Energy and the National Science Foundation. We also would like to acknowledge the partial support of the National Science Council of Taiwan and NTU-MOE.

[1] R. P. Madden and K. Codling, Phys. Rev. Lett. **10**, 516 (1963).
[2] For a recent review, see G. Tanner, K. Richter, and J. M. Rost, Rev. Mod. Phys. **72**, 497 (2000).
[3] O. Marchuk, G. Bertschinger, H.-J. Kunze, N. R. Badnell, and S. Fritzsche, J. Phys. B **37**, 1951 (2004).
[4] J. R. Harries, J. P. Sullivan, J. B. Sternberg, S. Obara, T. Suzuki, P. Hammond, J. Bozek, N. Berrah, M. Halka, and Y. Azuma, Phys. Rev. Lett. **90**, 133002 (2003).
[5] C. Såthe, M. Strom, M. Agaker, J. Soderstrom, J. E. Rubensson, R. Richter, M. Alagia, S. Stranges, T. W. Gorczyca, and F. Robicheaux, Phys. Rev. Lett. **96**, 043002 (2006).
[6] K. C. Prince, M. Coreno, R. Richter, M. DeSimone, V. Feyer, A. Kivimaki, A. Mihelic, and M. Zitnik, Phys. Rev. Lett. **96**, 093001 (2006).
[7] M. Alagia, M. Coreno, H. Farrokhpour, P. Franceschi, A. Mihelič, A. Moise, R. Omidyan, K. C. Prince, R. Richter, J. Söderström, S. Stranges, M. Tabrizchi, and M. Žitnik, Phys. Rev. Lett. **102**, 153001 (2009).
[8] A. Mihelič and M. Žitnik, Phys. Rev. Lett. **98**, 243002 (2007).
[9] K. T. Chung, T. K. Fang, and Y. K. Ho, J. Phys. B **34**, 165 (2001).
[10] X. M. Tong and C. D. Lin, Phys. Rev. Lett. **92**, 223003 (2004).
[11] J. Eiglsperger, B. Piraux, and J. Madronero, Phys. Rev. A **81**, 042527 (2010); **81**, 042528 (2010).
[12] S. I. Themelis, Phys. Scr. **83**, 045302 (2010).
[13] M. Žitnik, F. Penent, P. Lablanquie, A. Mihelic, K. Bucar, R. Richter, M. Alagia, and S. Stranges, Phys. Rev. A **74**, 051404(R) (2006).
[14] C. H. Yao and S. I. Chu, Chem. Phys. Lett. **204**, 381 (1993).
[15] J. Y. Wang, S. I. Chu, and C. Laughlin, Phys. Rev. A **50**, 3208 (1994).
[16] X. M. Tong and S. I. Chu, Chem. Phys. **217**, 119 (1997).
[17] X. Chu and S. I. Chu, Phys. Rev. A **63**, 023411 (2001).
[18] X. M. Tong and S. I. Chu, Phys. Rev. A **57**, 452 (1998).
[19] D. A. Telnov, J. Heslar, and S. I. Chu, Chem. Phys. **391**, 88 (2011).
[20] D. A. Telnov and S. I. Chu, Phys. Rev. A **83**, 063406 (2011).
[21] D. A. Telnov and S. I. Chu, Phys. Rev. A **79**, 041401(R) (2009).
[22] J. Heslar, J. J. Carrera, D. A. Telnov, and S. I. Chu, Int. J. Quantum Chem. **107**, 3159 (2007).
[23] J. Heslar, D. Telnov, and S. I. Chu, Phys. Rev. A **83**, 043414 (2011).
[24] S. I. Chu, J. Chem. Phys. **123**, 062207 (2005).
[25] For a review of generalized Floquet formalisms, see S. I. Chu and D. A. Telnov, Phys. Rep. **390**, 1 (2004).
[26] X. Chu and S. I. Chu, Phys. Rev. A **63**, 013414 (2000).
[27] X. M. Tong and C. D. Lin, Phys. Rev. A **71**, 033406 (2005).
[28] X. Guan, X. M. Tong, and S. I. Chu, Phys. Rev. A **73**, 023403 (2006).

[29] O. I. Tolstikhin, S. Watanabe, and M. Matsuzawa, J. Phys. B **29**, L389 (1996).
[30] A. Mehelic, Ph.D. thesis, Faculty of Mathematics and Physics, University of Ljubljana, 2006.
[31] A. Burgers, D. Wintgen, and J.-M. Rost, J. Phys. B **28**, 3163 (1995).
[32] G. Lagmago Kamta, B. Piraux, and A. Scrinzi, Phys. Rev. A **63**, 040502 (2001).
[33] J. Eiglsperger, M. Schönwetter, B. Piraux, and J. Madroñero, At. Data Nucl. Data Tables **98**, 120 (2012).
[34] J. M. Rost, K. Schulz, M. Domke, and G. Kaindl, J. Phys. B **30**, 4663 (1997).
[35] L. Lipsky and M. J. Conneely, Phys. Rev. A **14**, 2193 (1976).
[36] *Atomic, Molecular, and Optical Physics Handbook*, edited by G. W. F. Drake (AIP, New York, 1996).
[37] M. J. Seaton, Rev. Prog. Phys. **46**, 167 (1983).
[38] D. Wintgen, A. Bürgers, K. Richter, and G. Tanner, Prog. Theor. Phys. **116**, 121 (1994).
[39] Jan-Erik Rubensson (private communication).
[40] See, for example, E. Merzbacher, *Quantum Mechanics*, 3rd ed. (Wiley, New York, 1998).